Supplementary Information

Synergistic cooperation of PDI family members in peroxiredoxin 4-driven oxidative protein folding

Yoshimi Sato[1,6], Rieko Kojima[1,6], Masaki Okumura[1,5,6], Masatoshi Hagiwara[1,6], Shoji Masui[1,5], Ken-ichi Maegawa[1], Masatoshi Saiki[2], Tomohisa Horibe[3], Mamoru Suzuki[4] and Kenji Inaba[1,5]*

Supplementary Method

Plasmid construction

The *M. musculus* Prx4 (mPrx4) gene in pGEX5X-1 was kindly provided by Dr. Roberto Sitia (San Raffaele Scientific Institute, Milan). To prepare recombinant mPrx4 with a hexahistidine tag at the N-terminus, the mPrx4 gene lacking the signal sequence (residues 41–274) was subcloned into the *Nde*I-*Bam*HI site of vector pET15b. The C54A variant of full-length mPrx4 (C54A) was constructed using the Quick Mutagenesis Kit (Stratagene). To construct N-terminally truncated Prx4 (smPrx4), the DNA fragment encoding Leu79–Asn274 of mPrx4 was amplified by PCR and subcloned into the *Nde*I-*Bam*HI site of pET15b. The Prx4 derivative lacking the C-terminal 25 amino acids (Prx4 ΔC) was constructed by introduction of a stop codon immediately after Pro249.

The human P5 (Lys20–Leu440) and ERp57 (Ser25–Leu481) genes cloned into pET15b were a kind gift from Dr. Masakazu Kikuchi (Ritsumeikan University). The rat ERp72 gene cloned into pGEX-AT[41] was kindly provided by Dr. Tohru Kamata (Shinshu University). The DNA fragment encoding Ala21–Leu643 of rat ERp72 was amplified by PCR and subcloned into the *Nde*I-*Bam*HI site of pET15b. The human

ERp46 gene was amplified by PCR using the Human Pancreas QUICK-Clone cDNA library (Clontech Ltd.) as a template and cloned into pCR2.1-TOPO (Invitrogen Ltd.). The DNA fragment encoding Arg33–Leu432 of human ERp46 was amplified by PCR and cloned into the *Nde*I-*Bam*HI site of pET15b after site-directed mutagenesis to remove a *Bam*HI site in the coding region.

Vectors for overexpression of isolated Trx domains of human PDI (**a** and **a'**) were constructed by subcloning the coding regions (Asp18–Pro135 and Trp364–Gln475, respectively) into the *Nde*I-*Bam*HI site. For overexpression of isolated P5 $\mathbf{a^0}$ and $\mathbf{a^1}$ and ERp46 $\mathbf{a^2}$, DNA fragments containing the coding regions (Ser24–Leu129 and Ser154–Ala273 for P5 and Gly322-Leu432 for ERp46) were subcloned into the *Bam*HI-*Eco*RI site of pGEX-5X-1 (GE Healthcare). The coding regions for ERp46 $\mathbf{a^0}$ (Ser62–Glu170) and $\mathbf{a^1}$ (Gly190–Glu298) were subcloned into the *Nde*I-*Bam*HI site of the vector pOPTG. P5 $\mathbf{a^0}$ CXXA variant was constructed using the Quick Mutagenesis Kit (Stratagene) from the vector encoding P5 $\mathbf{a^0}$.

Protein expression and purification

Vectors were transformed into *Escherichia coli* BL21(DE3). Cells harboring plasmids for overexpression of mPrx4, PDIs, and their derivatives were grown at 30°C and induced by the addition of 0.5 mM IPTG at an OD_{600} of 0.5. Cells were incubated with agitation for 4 h at 30°C and then harvested. For overexpression of isolated PDI Trx domains, cells were grown at 15°C, induced with IPTG at an OD_{600} of 0.3, and incubated at 15°C for 18 h.

To purify mPrx4 and its derivatives, cells in buffer A (50 mM Tris-HCl, pH 8.1, and

0.3 M NaCl) containing 1 mM PMSF were disrupted using a microfluidizer (Niro Soavi PA2K). After clarification of the cell lysate by centrifugation at 12,000 rpm for 20 min, the supernatant was loaded on an open Ni-NTA Sepharose column (QIAGEN). The column was washed with buffer A containing 20 mM imidazole, and mPrx4 was eluted with buffer A containing 200 mM imidazole. The eluted sample was concentrated to 500 μl by filtration using Amicon Ultra filter units (MWCO, 50,000; Millipore), applied to a Mono-Q 10/100 anion exchange column (GE Healthcare) pre-equilibrated with 50 mM Tris-HCl (pH 8.1), and eluted with a linear gradient of 0–500 mM NaCl. To prepare fully oxidized mPrx4, diamide was added to purified mPrx4 at a final concentration of 10 mM, and the solution was incubated on ice for 30 min. The sample was loaded on a Superdex 200 10/300 size exclusion column (GE Healthcare), pre-equilibrated with buffer A containing 1 mM EDTA, to remove the diamide.

Purification of PDIs was carried out as previously described[15]. Briefly, the supernatant of the cell lysate was applied to the open Ni-NTA Sepharose column. Fractions eluted with 200 mM imidazole were further purified by anion exchange chromatography with a MonoQ column.

To purify GST-fused P5 $\mathbf{a^0}$ CXXA, the supernatant of the cell lysate was loaded on an open Glutathione Sepharose column (GE Healthcare). The column was washed with phosphate-buffered saline (PBS) and the sample was eluted with PBS containing 10 mM GSH. Samples were dialyzed against 1× Xa buffer (20 mM Tris, pH 8.0, 500 mM NaCl, and 50 mM $CaCl_2$) and digested with 1 U Factor Xa per mg protein at 20°C for 24 h. The digested product was separated by gel filtration on a Superdex 75 10/300

column in buffer A containing 1 mM EDTA.

Crystallization of mPrx4

For crystallization of mPrx4, its Cys54Ala mutant (C54A) was used. The mutant was concentrated to approximately 10 mg/ml and dialyzed against 20 mM HEPES (pH 7.0) containing 100 mM NaCl. Crystals of C54A appeared within one week with vapor diffusion at 20°C under conditions of 8%–10% polyethylene glycol (PEG) monomethyl ether 550 (PEG-MME550) and 50 mM MES (pH 6.5). For cryoprotection, the crystals of C54A was transferred directly to solutions of 15% PEG-MME550, 50 mM MES (pH 6.5) and 20% glycerol. Crystals were flash-frozen with cold nitrogen gas from a cryostat (Rigaku).

Supplementary figure legends

Supplementary Fig. S1. Activity of Prx4 and Ero1α toward PDIs *in vitro*

(A) SDS-PAGE analysis (reducing conditions) and Coomassie blue staining of purified recombinant PDIs used in this study.

(B) Schematic representation of the assay system used to assess the activity of Prx4 or Ero1α toward PDIs. Consumption of NADPH coupled to Prx4 or Ero1α catalysis was detected by monitoring absorbance at 340 nm (Abs_{340}).

(C) Prx4 activity toward PDIs. The decrease in Abs_{340} (upper) reflects the consumption of NADPH during the Prx4 catalysis of oxidation of PDIs. Conditions during the assay were as described in Materials and Methods of the main body. The bar graph (lower)

represents the rate of NADPH consumption, which was calculated by measuring the gradient in the initial linear phase of the decay curve of Abs_{340}. Values are the mean ± SD of three independent experiments.

(D) As in (C) except that the constitutively active mutant of human Ero1α (Cys104&131Ala) was incubated with PDIs instead of Prx4. The bar graph (lower) represents the rate of NADPH consumption calculated by measuring the gradient in the intermediate linear phase of the Abs_{340} decay curve.

Supplementary Fig. S2. Specific recognition of each Trx domain of P5 and ERp46 by Prx4

(A) Selective oxidation of isolated Trx domains $\mathbf{a^0}$ and $\mathbf{a^1}$ and CxxC mutants of P5 by Prx4. Consumption of NADPH coupled to Prx4 catalysis was detected by monitoring Abs_{340}. Conditions during the assay were as described in Materials and Methods of the main body.

(B) As in (A) except that isolated Trx domains and CxxC mutants of ERp46 were used instead of those of P5.

(C) Marginal oxidation of isolated Trx domains **a** and **a'** of PDI by Ero1α. Note that Ero1α oxidizes the PDI **b'a'c** fragment and the AXXA-CXXC variant more efficiently than isolated **a** and **a'**. Consumption of NADPH coupled to Ero1α catalysis was detected as in (A).

(D) As in (C) except that isolated Trx domains and CxxC mutants of ERp46 were used instead of PDI derivatives.

Supplementary Fig. S3. Full-length blots presenting the redox states of PDIs and Prx4 in wild-type or Prx4-overexpressing HEK293 cells pretreated with various concentrations of H_2O_2.

(A) Redox states of PDIs are visualized by immunoblotting the TCA precipitates of wild-type or Prx4-overexpressing HEK293 cells pretreated with various concentrations of H_2O_2, after the alkylation of free cysteines. The representative full-length gel images under non-reducing (left) and reducing (right) conditions of the three independent experiments are shown. The squares indicate the regions of interest that are highlighted in Fig. 1B of the main body. The comparison of the full-length blots under non-reducing and reducing conditions indicated that the large portion of endogenous PDI and ERp46 formed mixed disulfide complexes in cultured cells, regardless of the H_2O_2 addition and Prx4 overexpression. Endogenous P5 also formed mixed disulfide complexes in cultured cells, but in a manner dependent on H_2O_2 concentration.

(B) Redox states of endogenous (left) and exogenous (right) Prx4 are visualized by immunoblotting the TCA precipitates of wild-type or Prx4-overexpressing HEK293 cells pretreated with various concentrations of H_2O_2, after the alkylation of free cysteines. The representative full-length gel images under a reducing condition of the three independent experiments are shown.

(C) Comparison of the electrophoretic mobility of Mal-PEG-treated and -untreated PDIs on SDS gels. Note that Mal-PEG treatment significantly retarded the band

migration of PDI and ERp57, resulting in the increase of their apparent molecular weight. Accordingly, PDI and ERp57 contain two and one free cysteines outside the redox-active sites, respectively.

Supplementary Fig. S4. Association and dissociation curves generated by SPR analysis of the affinities of PDI-family member proteins (PDIs) for Prx4.

Wild-type Prx4 was immobilized on a biosensor chip, and PDIs at the indicated concentrations were injected as analytes in the presence of 1 mM GSH and 0.25 mM GSSG. Kinetic parameters that were calculated based on SPR analysis are shown in Fig. 2A.

Supplementary Fig. S5 Structural comparison of oxidized and reduced forms of mammalian Prx4

(A) Alignment of the amino acid sequences of human and mouse Prx4. "*" and ":" below the sequence indicate that the residues in those columns are completely identical and highly similar between these two, respectively. The peroxidatic and resolving cysteines are marked by red and blue arrows, respectively. Note that the Prx4 from *Mus musculus* (mPrx4) shows 96% identity and 99% homology to Prx4 from *Homo sapiens* (hPrx4) at the amino acid sequence level, except for the amino acid sequence of the signal sequence (supplementary Fig. S4A).

(B) Crystal structure of oxidized Prx4 from *Mus musculus* (mPrx4) at 3.3 Å resolution. Upper (left) and side (right) views of the decameric structure of mPrx4 are represented

by a ribbon diagram.

(C) Superposition of oxidized forms of mPrx4 and human Prx4 (hPrx4) with the minimized RMSD of their Cα atoms.

(D) Crystal structures of a dimeric unit in mPrx4 decamer in the oxidized state (left) and in hPrx4 decamer in the reduced state (right) are shown by a ribbon representation. Dotted lines in the oxidized form indicate the C-terminal region for which electron density was undetectable, presumably due to the extreme flexibility of this region. Redox-dependent structural changes around the active-site cysteines are highlighted in insets.

Supplementary Fig. S6 Full-length gels presenting the time course of oxidation of reduced and denatured RNase A catalyzed by the Prx4-PDIs combinations. The squares indicate the regions of interest that are highlighted in Fig. 4A of the main body. Note that covalently linked Prx4 oligomers were little detected because they were out of the detection range of the used non-reducing SDS gels (15 %).

Supplementary Fig. S7 Oxidative folding of RNase A catalyzed by PDIs and H_2O_2 but in the absence of Prx4. Reduced and denatured RNase A (25 μM) was refolded for the indicated times by the indicated PDIs (2 μM) in buffer (pH 7.5) containing H_2O_2 (100 μM) without Prx4. The reaction was quenched by cysteine alkylation with AMS, and the generated species were resolved by non-reducing SDS-PAGE. Labels Red., PO, and Oxd. denote fully reduced, partially oxidized, and fully oxidized RNase A,

respectively.

Supplementary Fig. S8 Marginal synergistic effect for ERp46 and P5 in the Prx4-driven oxidative folding of RNase A Time course of the oxidative folding of reduced and denatured RNase A (25 μM) catalyzed by Prx4 (0.2 μM), P5 (2 μM), and ERp46 (2 μM) in buffer (pH 7.5) containing H_2O_2 (100 μM). The redox state of RNase A was monitored by non-reducing SDS-PAGE in a 15% gel after cysteine alkylation with AMS (left). The recovery of RNase A activity was measured spectrophotometrically by the change in Abs_{295} using cCMP as a substrate (right). Values are the mean ± SD of two independent experiments.

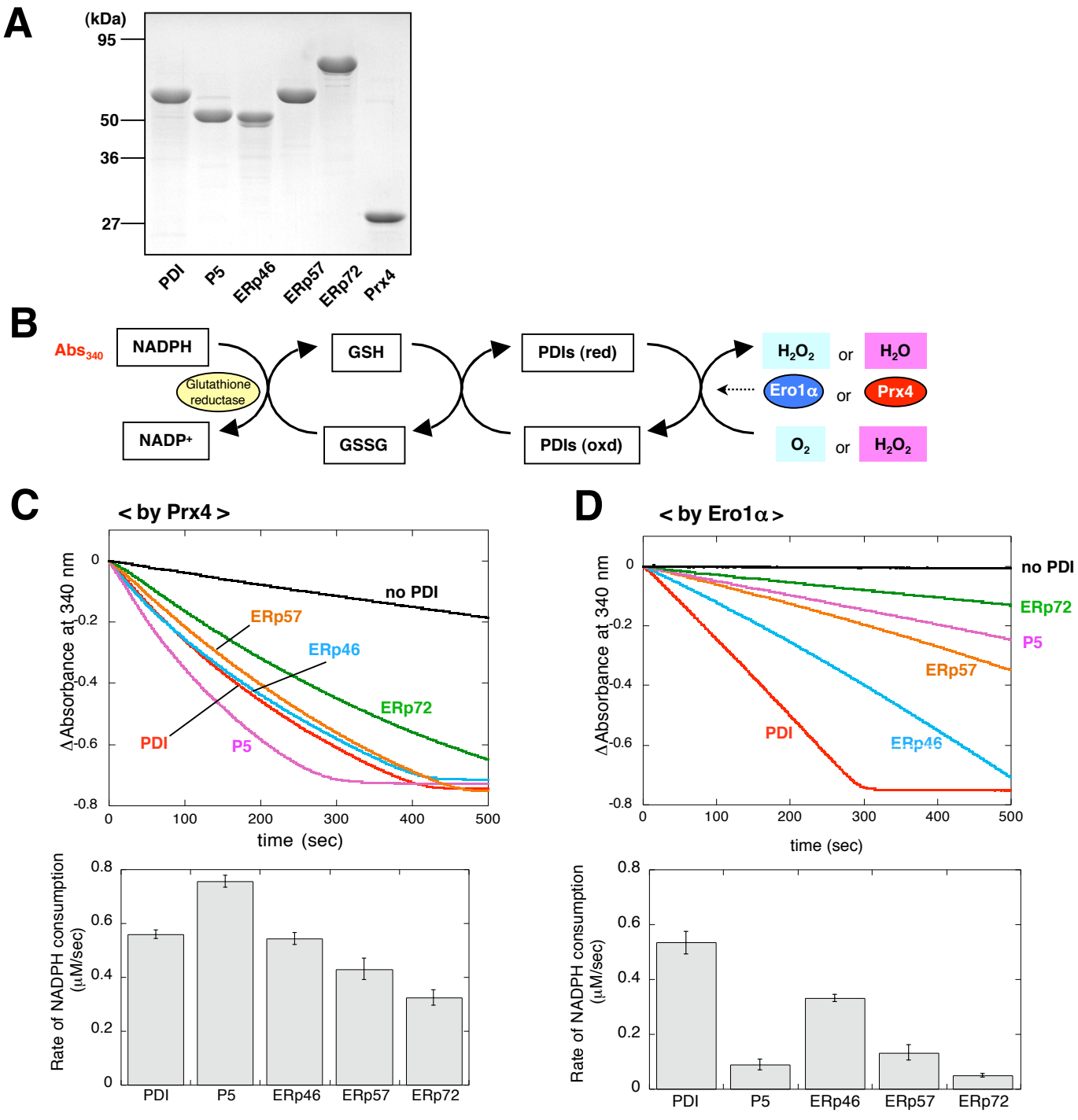

Supplementary Fig. S1

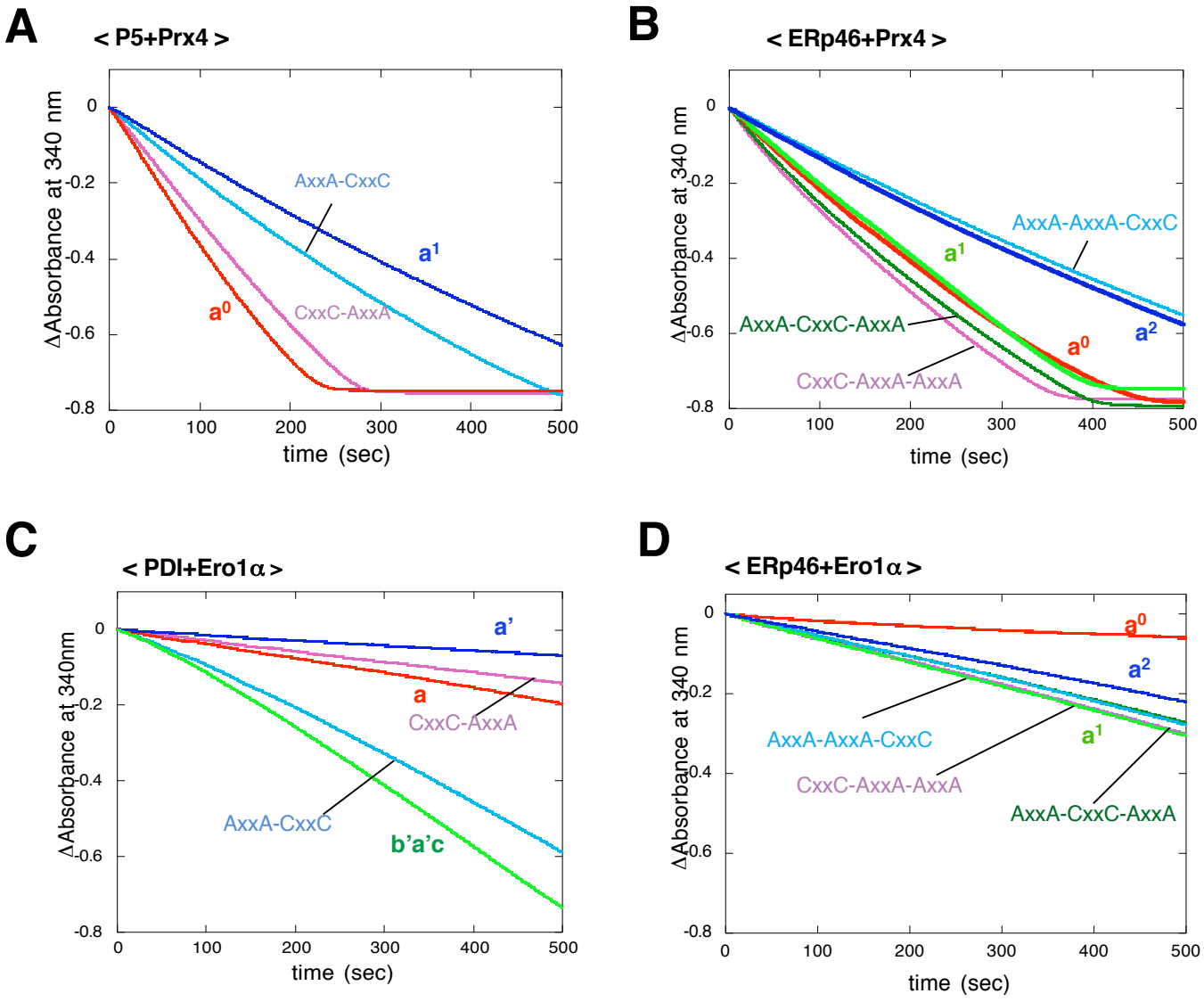

Supplementary Fig. S2

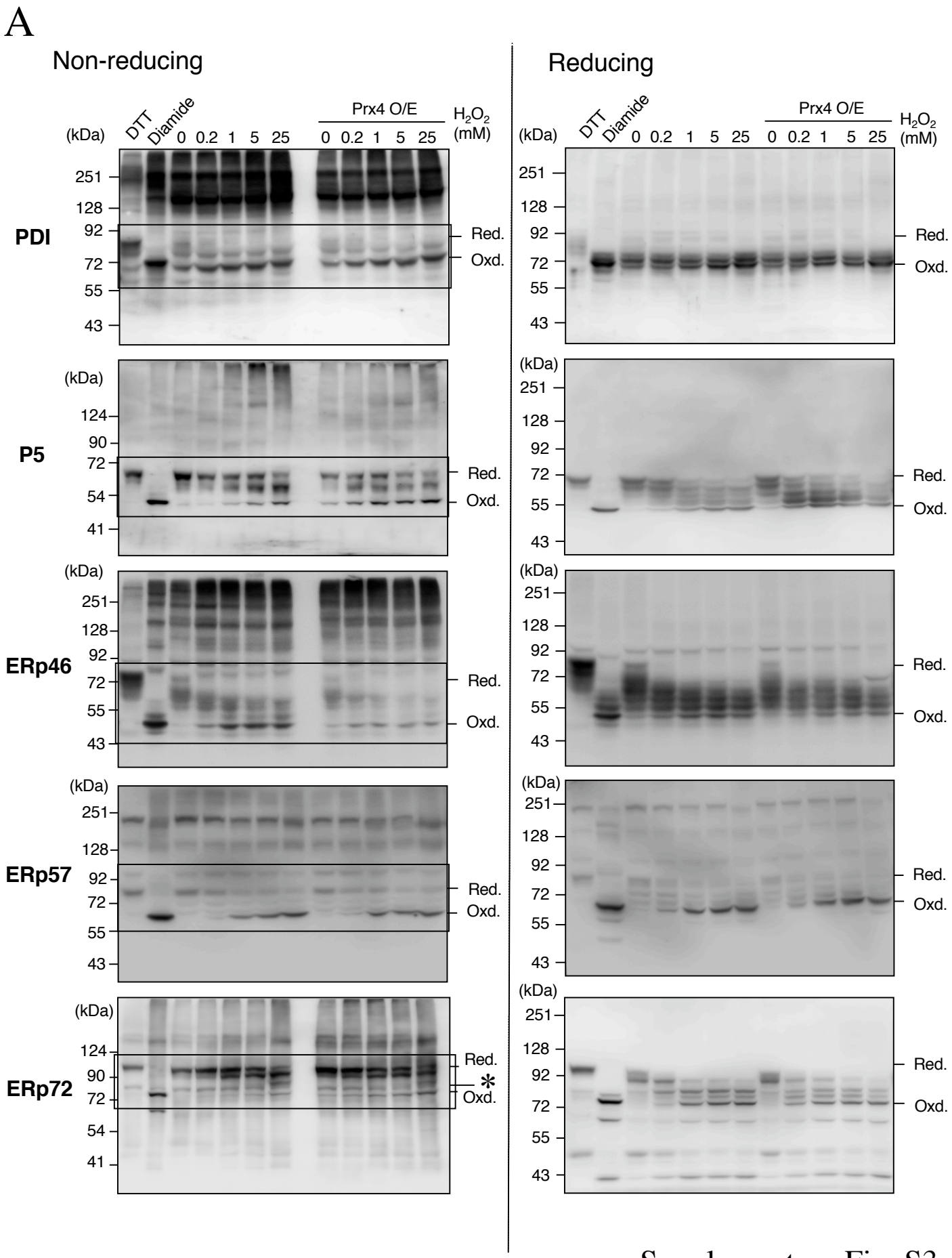

Supplementary Fig. S3

B

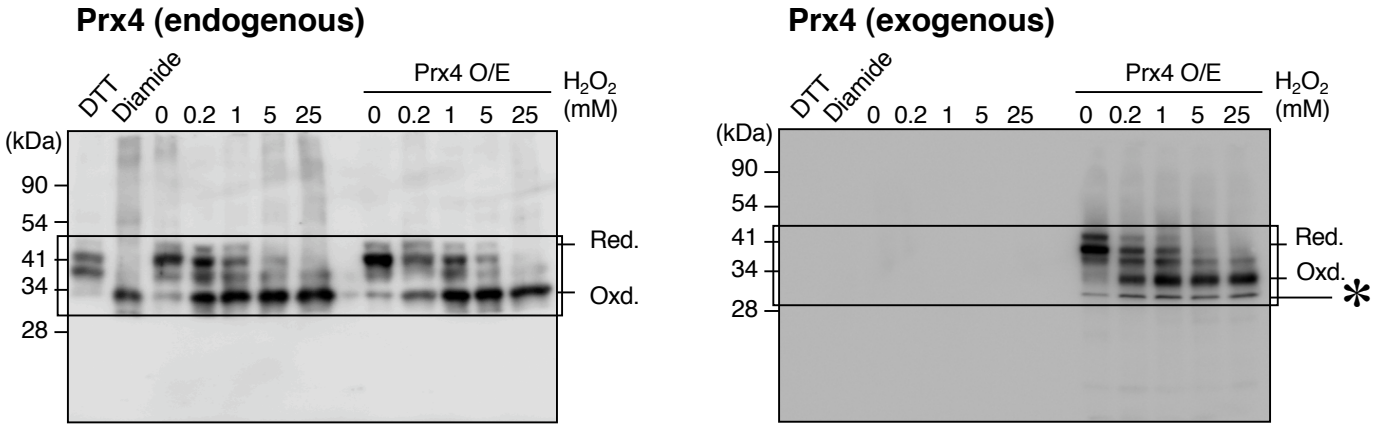

C

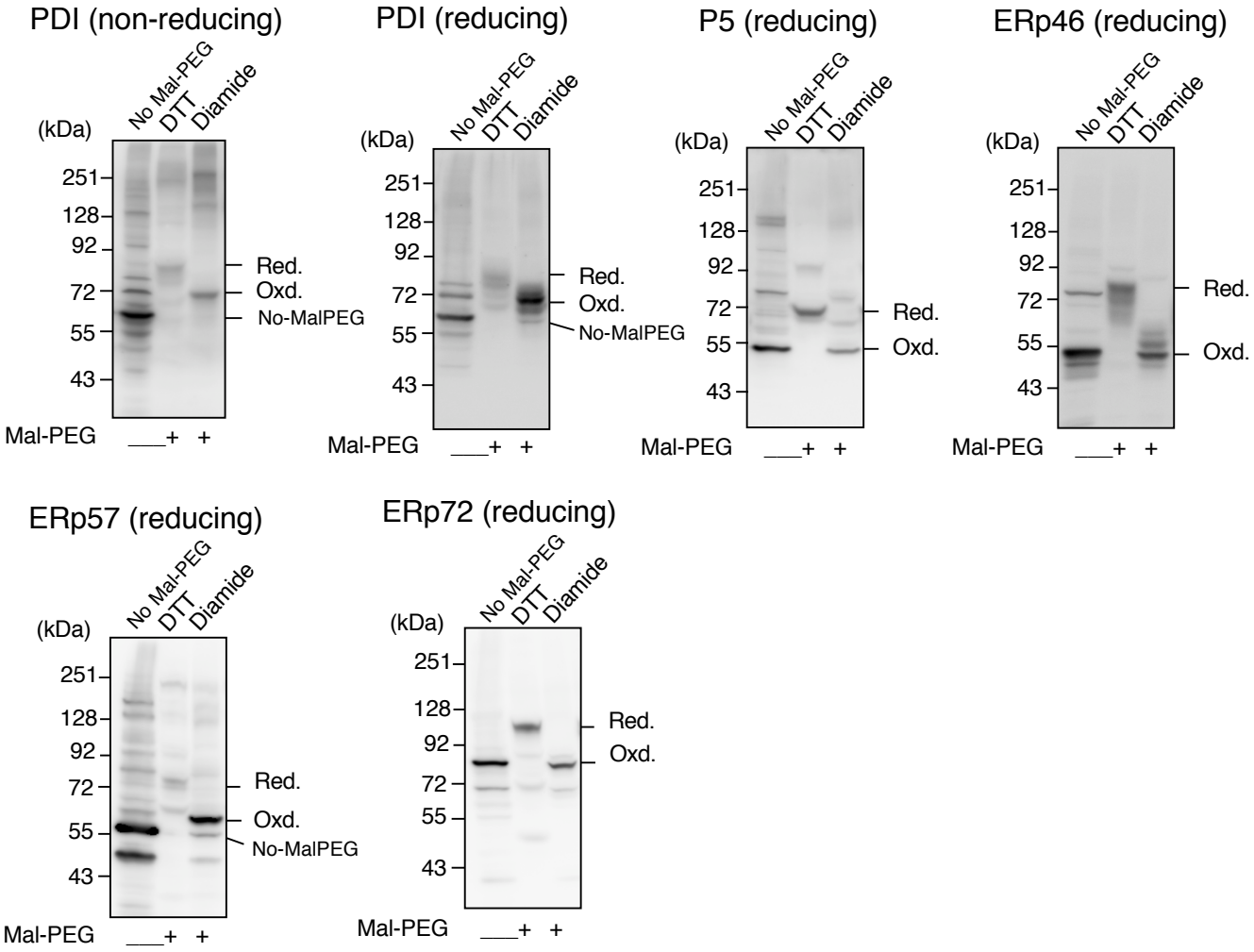

Supplementary Fig. S3

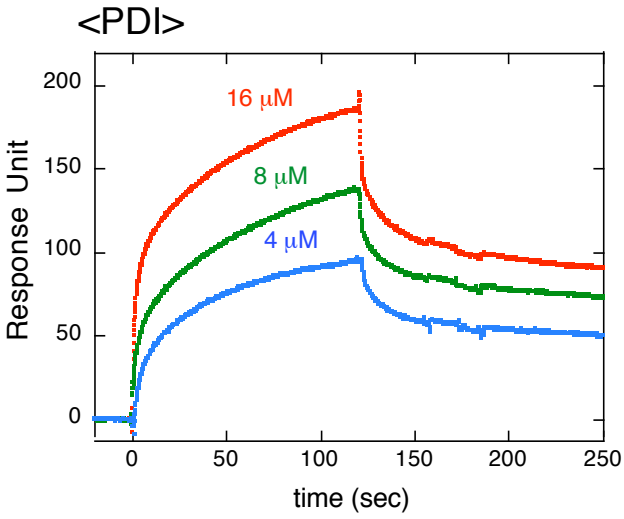

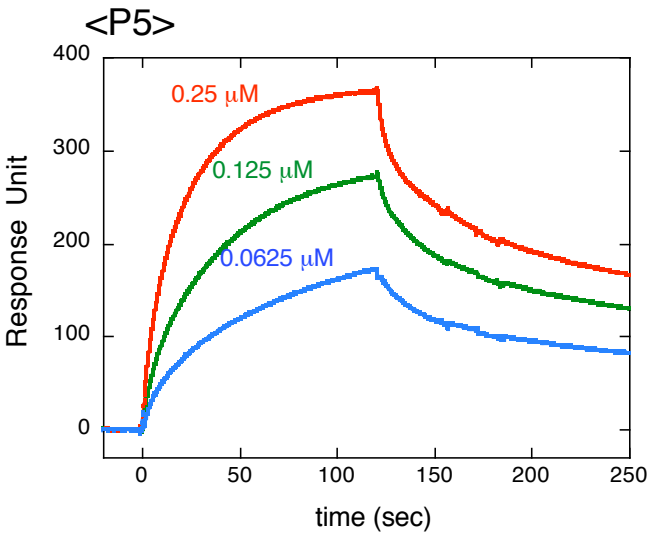

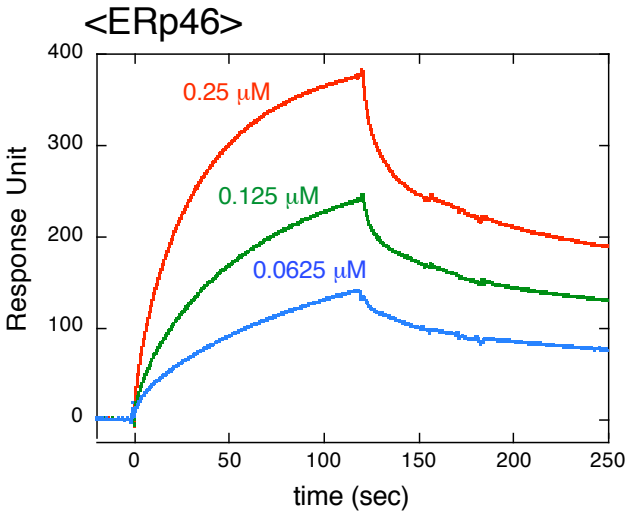

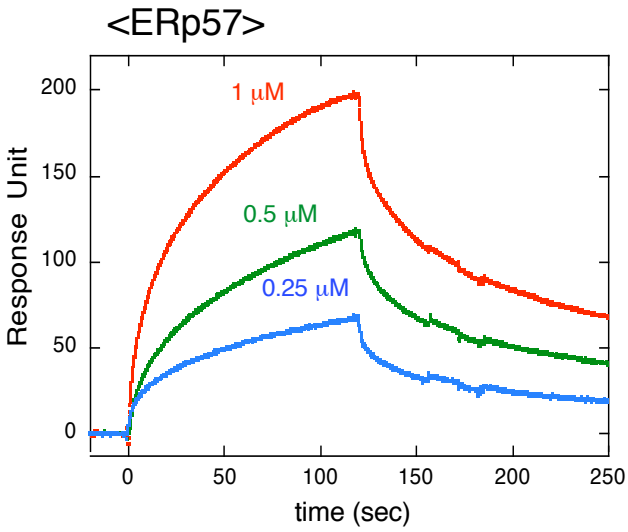

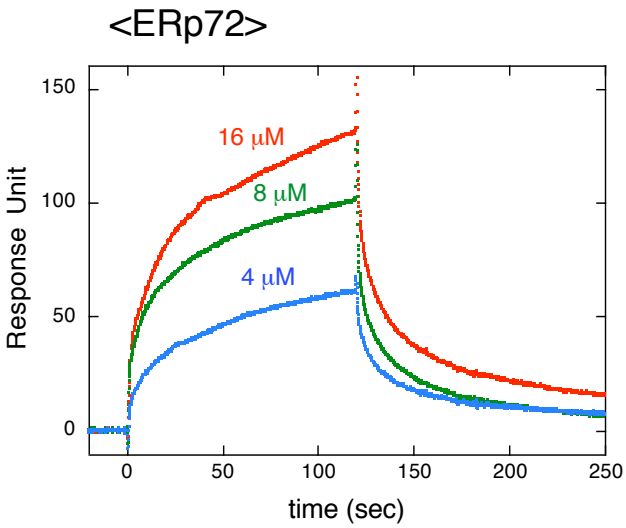

Supplementary Fig. S4

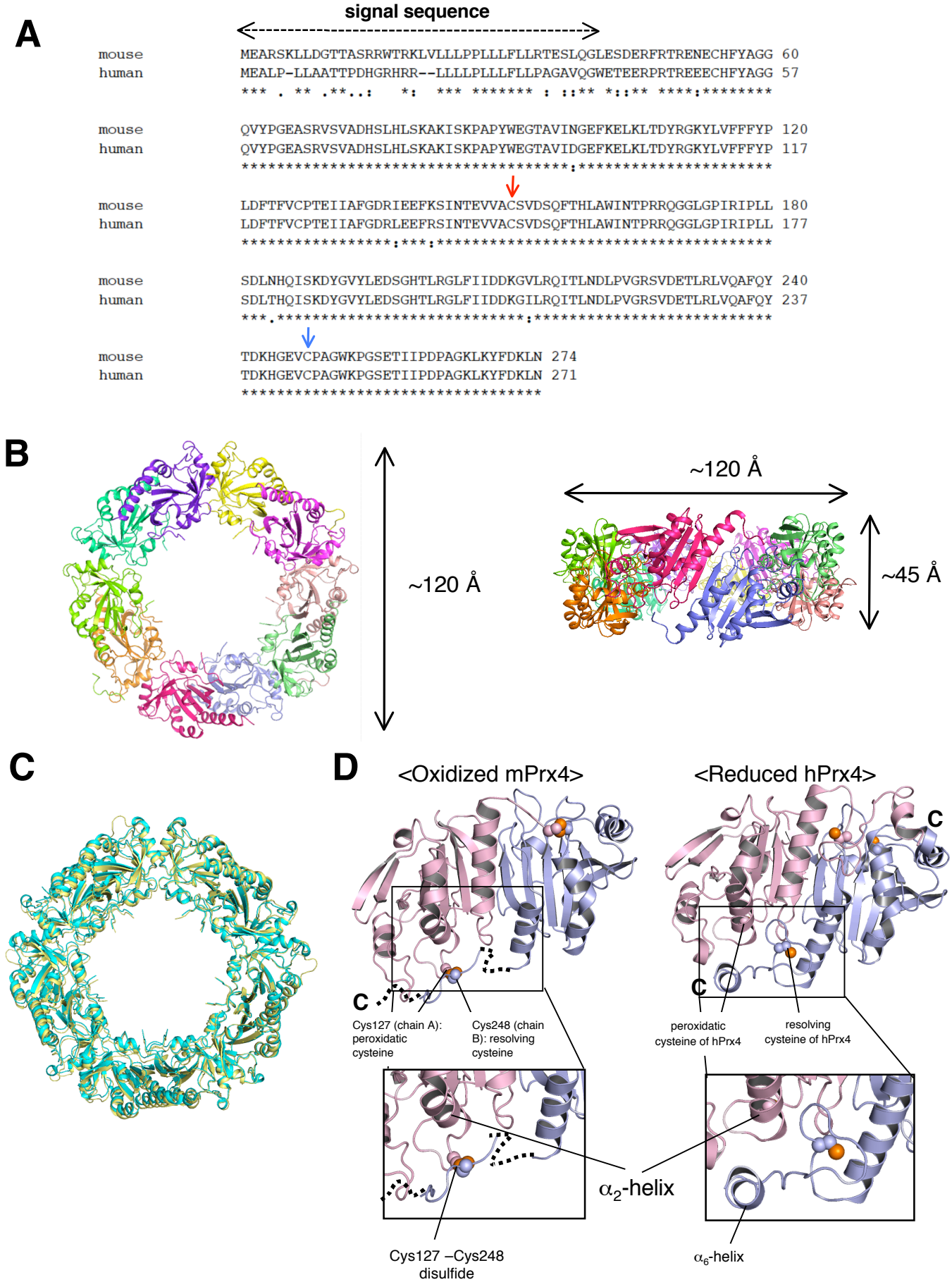

Supplementary Fig. S5

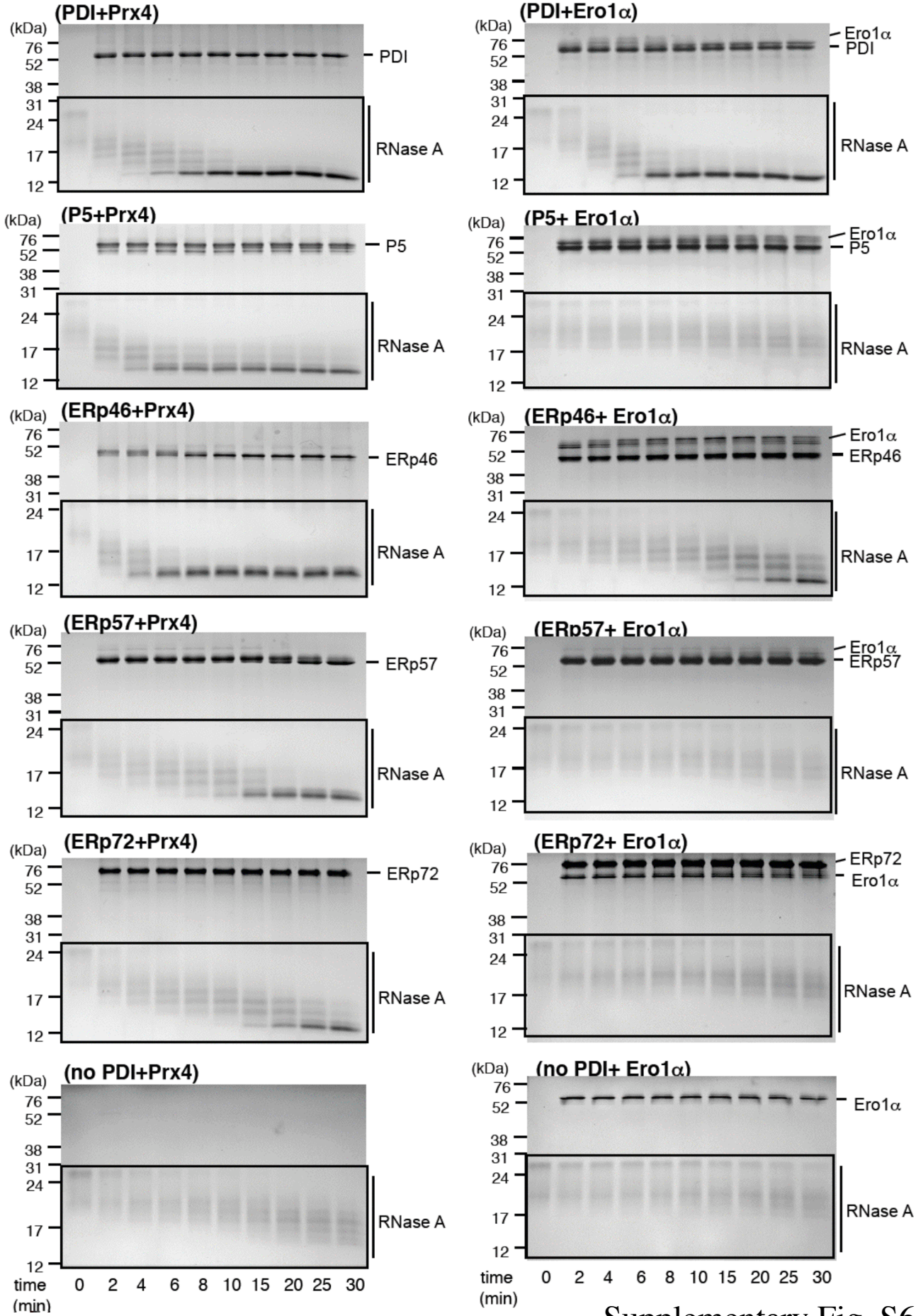

Supplementary Fig. S6

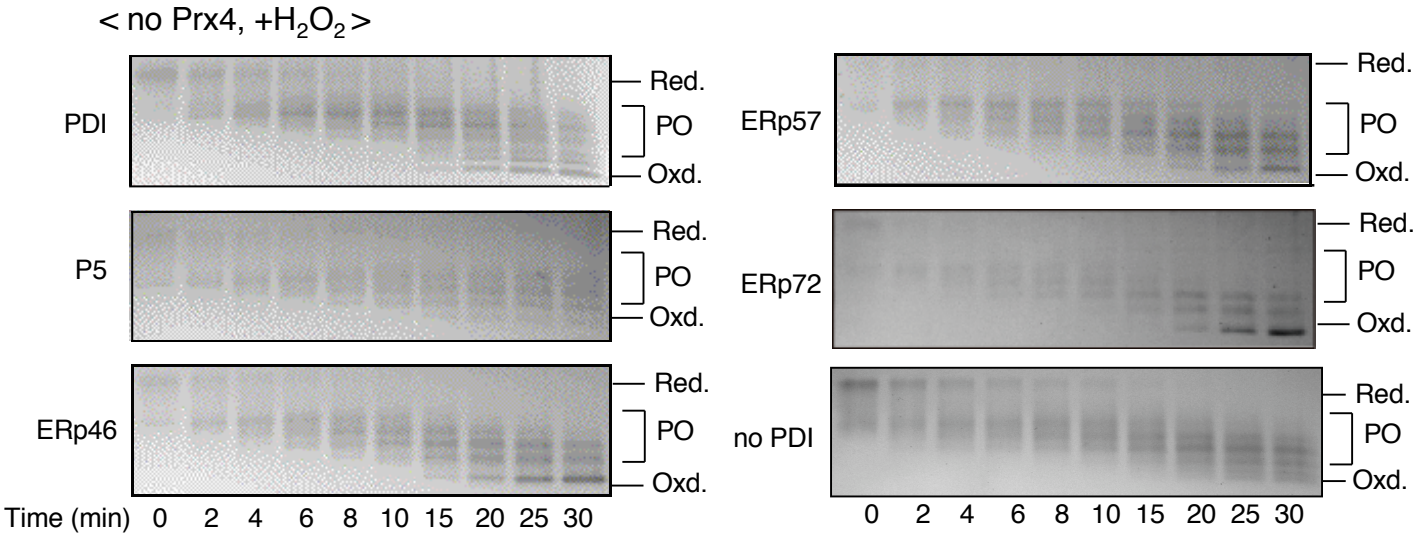

Supplementary Fig. S7

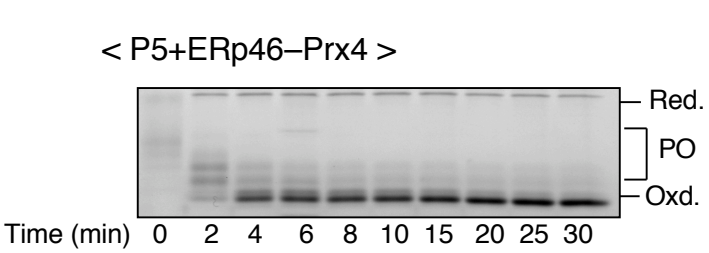

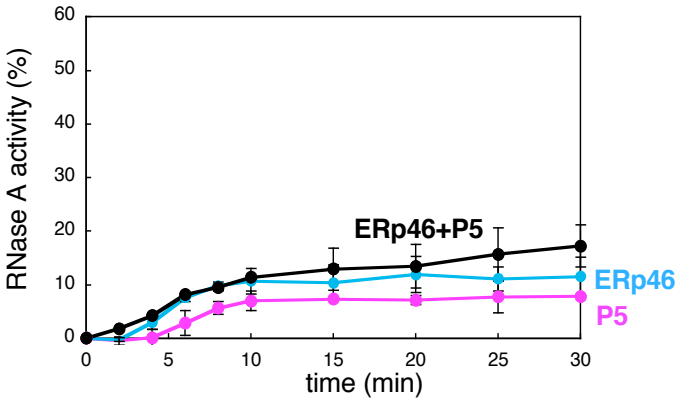

Supplementary Fig. S8